International Journal of Heat and Mass Transfer 52 (2009) 6050–6058

Contents lists available at ScienceDirect

International Journal of Heat and Mass Transfer

journal homepage: www.elsevier.com/locate/ijhmt

Static research of flow in rotor channels of the regenerator

Bogumił Bieniasz *

Thermodynamics Department, Rzeszów University of Technology, al. Powstańców Warszawy 8, 35-959 Rzeszów, Poland

ARTICLE INFO

Article history:
Received 16 January 2009
Received in revised form 13 March 2009
Accepted 18 May 2009
Available online 4 September 2009

Keywords:
Rotary regenerator
Pulsating flow
Electrolytic technique
Mass transfer

ABSTRACT

One demonstrates here the results of static experiments which suggest the pulsating flow in rotating channels of the rotor of heat regenerators occurs. Electrolytic technique was used to measure distribution of the mass transfer coefficient for one of many straight, round, radial ducts of the rotor for different angle positions at mean Reynolds number as a parameter. The use of the Chilton–Colburn analogy made it possible to state the angle-distribution of flow-velocity. The Reynolds number deviation was about ±30% in comparison with its mean value which suggests that the phenomenon should be taken into account in formulating the models of rotary heat exchangers. An equality – approximately – of the mean velocity of an out-gassed electrolyte in the opposite ducts of the rotor of the model, working in a closed hydraulic system, was stated which was justified theoretically for one-dimensional flow.

1. Introduction

The literature offers a lot of research information on the intensity of heat and mass transfer and of hydrodynamic phenomena of pulsating flow but only in the case of fixed channels, e.g. [1–5]. The papers concern the pulsation generated by artificial means and it was known in advance that they would occur. Contrary to these, this work would deal with the flow pulsation in the ducts of the rotor of the heat regenerator. This was due to a change of flow resistance of fluid with an angle position of the duct axis which takes place during rotation.

The high speed rotary heat regenerator may be used in many applications such as: ventilation of different rooms, workshops, swimming-pools, gymnasiums, houses, preheating of air for boiler furnaces, combustion chambers of turbo-gas power plants and turbine engines etc. Its advantage is small weight per unit thermal power.

It consists (Fig. 1) of porous rotor with fixed ordinary or broken partition inside of it and the casing. The angle between the two wings of the partition depends on main dimensions, angular velocity of the rotor, and properties of fluids. The rotor is driven from outside, which causes suction and forcing action, in relation to both hot and cold gas, similarly as in the case of a ventilator or centrifugal compressor. Small values of a hydraulic diameter result in small values of Reynolds number, characteristic for laminar flow.

The task of the regenerator is to recover the part of energy of the used warm gas and to utilise it to preheat the fresh, cold gas. Both gases flow into the regenerator through the suction branches coaxially due to counter flow mode. Assuming that there is sufficient leaktightness between the frontal surface of the rotor and that the casing exists, gases flow through every pore (channels, ducts) in general direction from the inside to the outside. Warm gas of the inlet temperature T_{H1} flows through the rotating porous rotor. It warms up the part of it being cooled to the temperature T_{H2} at the outlet of the regenerator. During a subsequent turn of the rotor its warmed material warms up the cold gas flowing through the channels in the next angular sector, from T_{C1} to T_{C2} at the outlet of the delivery branch.

A value of the ordinary partition-angle setting Φ – Fig. 1 – should prevent the mixing of the both gases to take place. For example, the cold gas entering the duct of the rotor at an angle equal to Φ should leave it at angle $\Phi = 0$. In a general case of non-radial ducts

$$\Phi = \Phi' - \Delta\Phi, \tag{1}$$

where $\Delta\Phi$ is known.

The Φ' means the angle distance of the rotor, moving with angular velocity ω, which is to be covered in time t of gas flow with a mean velocity w through the duct of length L.

Therefore

$$\Phi' = \omega t = \omega L/w = 2\pi\dot{n}_o L/w. \tag{2}$$

The appropriate path of the gas particles is shown in Fig. 1 as well as for the opposite and middle position.

The flow resistance at a distance from the point of departure to any cross-section of delivery branch A' for particles starting at point E is greater than that at G, the latter being next greater than that at D. It is obvious that – for fixed pressure drop for gas between suction branch and delivery branch-this must result in

* Tel.: +48 17 8628149; fax: +48 17 8543116.
E-mail address: bogubien@prz.edu.pl

0017-9310/$ - see front matter © 2009 Elsevier Ltd. All rights reserved.
doi:10.1016/j.ijheatmasstransfer.2009.05.012

Nomenclature

A	cross-section area of the duct, m^2
A_{cath}	working surface area of cathode, m^2
b	barometric pressure, $N\,m^{-2}$
C	rotameter constant
C_b	bulk concentration of ferricyanide ions, 10^{-3} N V_t/V_s, $kmol\,m^{-3}$
D	diffusivity of ferricyanide ions, $m^2\,s^{-1}$
d	diameter of radial duct, m
F	Faraday constant
h	depth beneath the liquid level, m
h_D	mass transfer coefficient, mean over the surface area of cathode, $m\,s^{-1}$
I	current in the circuit, A
I_p	plateau current, A
j_M	Chilton–Colburn mass transfer coefficient
k	number of the ducts of the rotor model
L	length of the duct, m
l_f	specific friction work, $J\,kg^{-1}$
N	normality of solution of $Na_2S_2O_3$ used as titrant
n	valence change of reacting ions
$\dot{n}_o$	rotational speed, s^{-1}
p	pressure
Re	Reynolds number, wd/ν
r	radius, m
Sc	Schmidt number, ν/D
Sh	Sherwood number, $h_D d/D$
St_M	mass transfer Stanton number, h_D/w
T	gas temperature, K
U	input voltage between anode and cathode, V
$\dot{V}$	volume flow rate of electrolyte, $C\dot{V}_r$, $m^3\,s^{-1}$
$\dot{V}_r$	volume flow rate of electrolyte indicated by rotameter, $m^3\,s^{-1}$
V_s	volume of electrolyte sample, ml
V_t	volume of titrant added, ml
w	velocity of fluid in the duct, $m\,s^{-1}$
$\bar{w}$	mean velocity of fluid in the duct over the whole rotor, $\dot{V}/(kA)$, $m\,s^{-1}$
z	position over the reference level, m

Greek symbols

α	angle setting of the cathode, rd
ς	relative deviation of the mass transfer coefficient for opposite ducts, (39)
μ	dynamic viscosity, $kg\,m^{-1}\,s^{-1}$
ν	kinematic viscosity, $m^2\,s^{-1}$
ξ	deviation of Reynolds number, (37)
ρ	density of fluid, $kg\,m^{-3}$
Φ	partition-angle setting, rd
ω	angular velocity of the rotor, $rd\,s^{-1}$

Subscripts

1, 2	inlet and outlet, respectively
b	bulk
c	cross-section
D	diffusion
el	electrolyte
H, C	hot and cold, respectively
i, o	inner and outer, respectively
p	plateau
r	rotameter
s	sample of electrolyte
t	titrant
u, l	upper and lower, respectively

Superscripts

i	successive value of parameter Re
j	kind of mutual orientation of manifolds
', ''	for primary and secondary orientation of manifolds, respectively

angular distribution of gas-velocity in the ducts of the rotor of the regenerator. Pulsating flow for the given rotating duct must occur, which in consequence will be the reason of angle-pulsation of convectional heat transfer coefficient value.

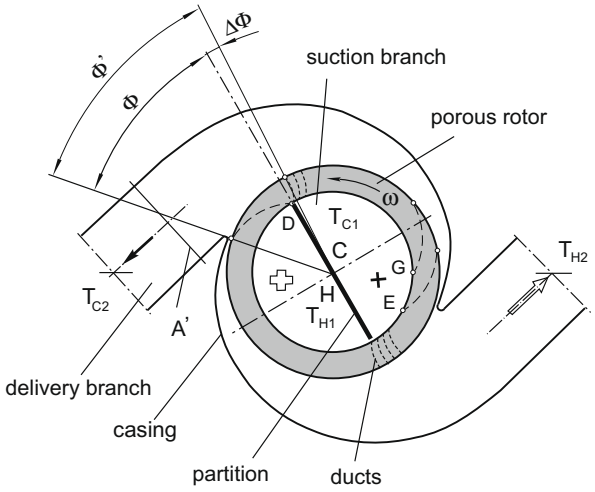

Fig. 1. Simplified scheme of the model of rotary heat regenerator.

Appropriate measurements for running a regenerator seem to be extremely difficult. Therefore, only the results of research for stationary conditions which, although roughly, indicate the scale of the problem, are being presented here.

2. Experiments

Electrolytic technique used in experiments was the same as described and detailed in [6]. The rig was also the same in general. The main elements of the rig are seen in the scheme shown in Fig. 2. There was no need of driving the rotor for static measurements. However the test section made it possible for the rotor-angle setting to be changed and recorded. Test section was the model of regenerator. The two arms of the manifold at the inlet of the model were symmetric. This assured that the equal flow- resistance for electrolyte entering the rotor axially from opposite sides of the suction branch and symmetry of velocity distribution towards the middle plane perpendicular to the rotor-axis to exist. The arms of manifolds at the outlet of the model were also symmetric for equality of electrolyte flow-rate in both delivery branches.

2.1. Model of regenerator

The main dimensions of the model casing are shown in Fig. 3. The casing was made from acid resistant steel 1H18N9T. To the inside

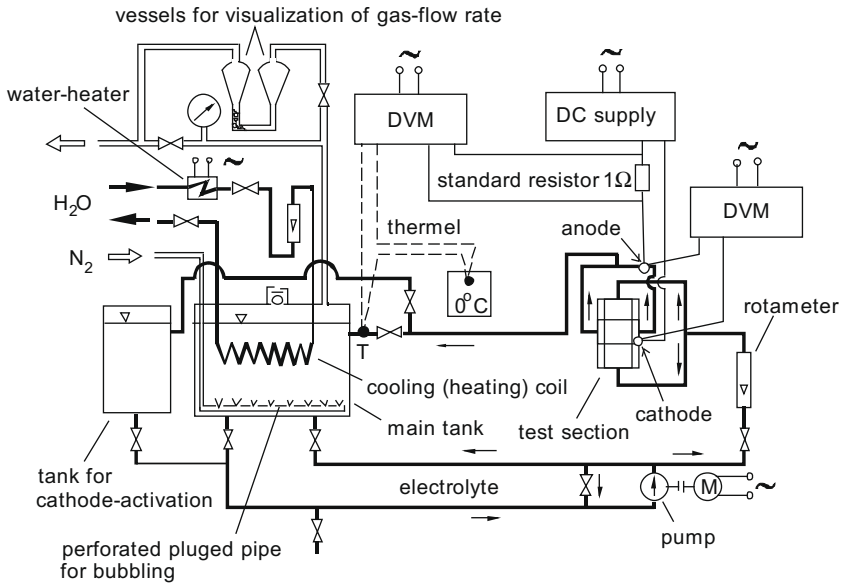

Fig. 2. Scheme of the rig.

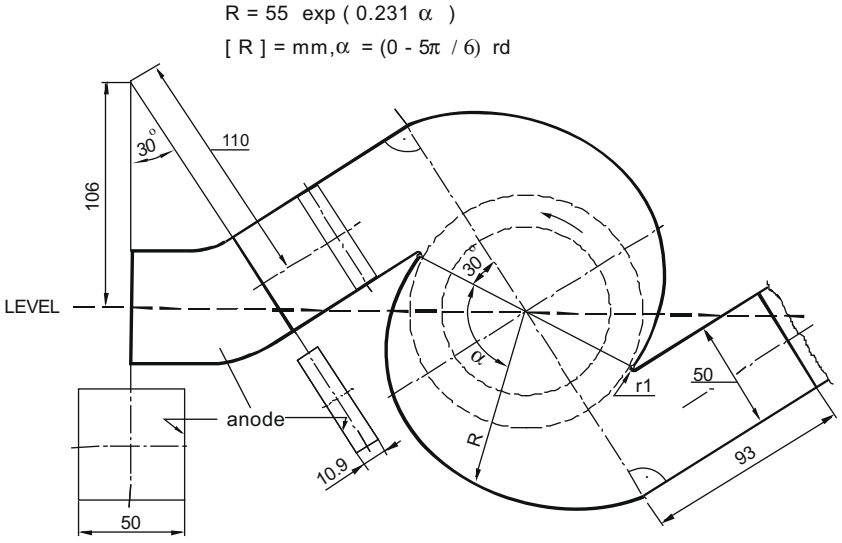

Fig. 3. Main dimensions of the casing of the model.

surfaces of both right-angle in cross-section elbows, being extensions of the delivery branches, sheets of fine nickel plate were glued. They were electrically isolated from the casing and connected parallel with themselves serving as a down-stream anode. The length of the casing in axis direction corresponds with the length of the rotor, presented in Fig. 4. The latter was correlated with the maximum volume-flux of electrolyte to be achieved on the rig for getting reasonable values of the Reynolds number in ducts of the rotor.

The rotor was made from PVC. It could be angular positioned with help of three rods passing the cut-outs spaced uniformly on a circumference. Six hundreds holes ϕ 1.5 $\times$ 15 mm were radially drilled on the basis of uniform perpendicular-mesh grid in fife planes situated symmetric to symmetry plane of the rotor. The four holes, uniformly situated in the symmetry plane, as shown in the revolved section, were provided with fine nickel bushes of the inner diameter and the length of all the holes. They could serve as cathodes during measurements. The cathodes, marked with roman numerals, were angularly positioned as shown in the figure.

No partition was used inside the rotor, which – together with the casing-was mounted in the middle of test section, shown schematically in Fig. 5, designed primarily for carrying on experiments with rotation. The test section enabled an identification of the angle position of selected cathode. Cross-sections of outlets from both delivery branches were situated on the same hydrostatic level only for convenience. It is worth to mention that the volume-fluxes of electrolyte through both symmetric delivery branches, being the parts of closed hydraulic system of the rig, are equal to themselves and are independent of the values of ordinate of centres of outlet cross-sections.

2.2. Distribution of the electrolyte entering the rotor of the model of regenerator on two volume-fluxes

The electrolyte with temperature of 20 °C and density 1040 kg m^{-3} was used in the research whereas the density of gases in the working regenerator was considerably lower, e.g. the density

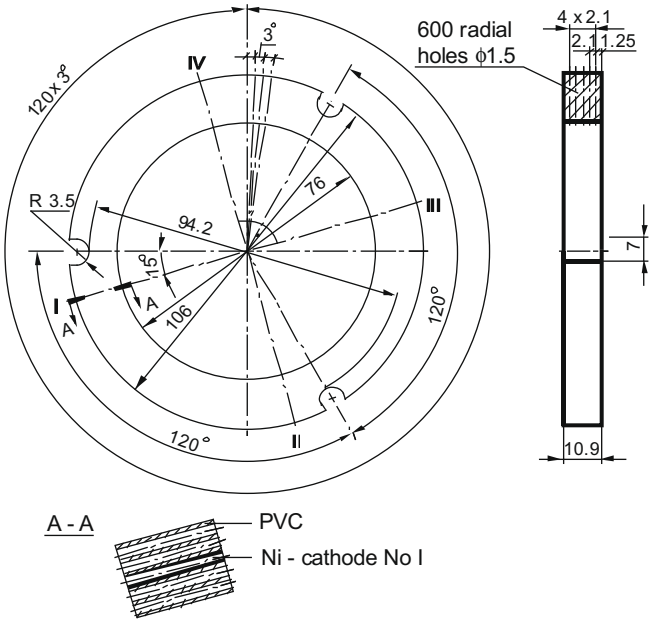

Fig. 4. Rotor.

of air of the same temperature and of the pressure of 1 atm equals to 1.205 kg m^{-3}. One may suspect that at horizontal axes of the model, Fig. 1, the volume-flux of electrolyte through the upper delivery branch will differ from that of the lower one. In such a case one could easily question full applicability of results of electrolytic measurements in designing of gas regenerators, where the hydrostatic effects, if present, might be neglected because of low density of gases.

One may compare the values of outlet velocity of liquid, pumped through the immovable rotor entirely immersed in the same liquid, Fig. 6, in the case of two ducts: upper *u*- and lower *l*-one.

Let the pressure of the liquid in the axes of horizontal rotor of radius r_i, equals to p_e at the level $z = e$. The pressure of liquid at the outlet from the upper duct *u* issues also from its hydrostatic pressure to a depth of h_{ou} beneath the liquid level:

$$p_{ou} = b + g\rho h_{ou} \tag{3}$$

Similarly one may assume that the liquid pressure at the outlet from the lower duct l, at the point *ou* ensues from its hydrostatic pressure to a depth of $h_{ou} + 2r_o$;

$$p_{ol} = b + g\rho(h_{ou} + z_{ou} - z_{ol}) \tag{4}$$

A pressure at the point *iu* is lower than p_e because of a head equal to r_i;

$$p_{iu} = p_e + -g\rho_(z_{iu} - z_{il})/2 \tag{5}$$

Next a pressure at the point *il* is greater than p_e because of the head r_i too;

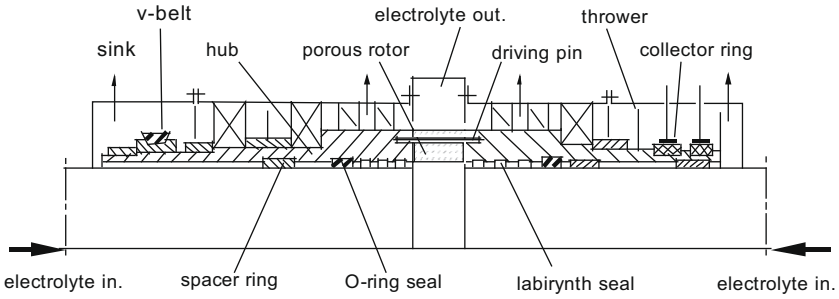

Fig. 5. Scheme of the test section.

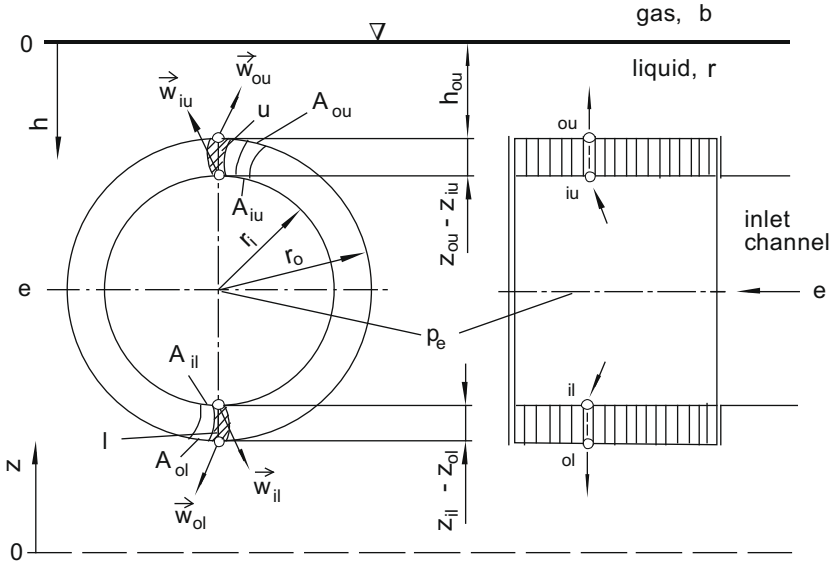

Fig. 6. Outflow of the liquid from the upper- and lower duct of the rotor.

$$p_{il} = p_e + g\rho(z_{iu} - z_{il})/2 \tag{6}$$

For one-dimensional adiabatic flow of the ideal liquid ($l_{fu} = l_{fl} = 0$), in homogeneous field of gravitational force, an energetic equation is of form of the Bernoulli theorem:

- for the duct u

$$\frac{w_{ou}^2 - w_{iu}^2}{2} + g(z_{ou} - z_{iu}) + \frac{p_{ou} - p_{iu}}{\rho} = 0 \tag{7}$$

- for the duct l

$$\frac{w_{ol}^2 - w_{il}^2}{2} + g(z_{ol} - z_{il}) + \frac{p_{ol} - p_{il}}{\rho} = 0 \tag{8}$$

The increments of a specific pressure energy, which occur in (7) and (8), are respectively:

- on the basis of (3) and (5)

$$\frac{p_{ou} - p_{iu}}{\rho} = K + g(z_{iu} - z_{il})/2 \tag{9}$$

- on the basis of (4) and (6)

$$\frac{p_{ol} - p_{il}}{\rho} = K + g(z_{ou} - z_{ol})/2 - g(z_{iu} - z_{il})/2 \tag{10}$$

where

$$K = b/p + gh_{ou} - p_e/\rho \tag{11}$$

The sum of the increment of specific potential energy and specific pressure energy:

- for duct u with consideration of (9) equals to

$$g(z_{ol} - z_{iu}) + \frac{p_{ou} - p_{iu}}{\rho} = K + g(z_{ou} - z_{ol})/2, \tag{12}$$

- for duct l with consideration of (10) equals to

$$g(z_{ol} - z_{il}) + \frac{p_{ol} - p_{il}}{\rho} = K + g(z_{ou} - z_{ol})/2, \tag{13}$$

because $z_{iu} + z_{il} = z_{ou} + z_{ol}$.

The Bernoulli law assumes the shape of, respectively:

- on the basis of (7), (12), and (11):

$$\frac{w_{ou}^2 - w_{iu}^2}{2} = \frac{p_e}{\rho} - \left[\frac{b}{\rho} + gh_{ou} + \frac{g(z_{ou} - z_{ol})}{2}\right] \tag{14}$$

- on the basis of (8), (13), and (11):

$$\frac{w_{ol}^2 - w_{il}^2}{2} = \frac{p_e}{\rho} - \left[\frac{b}{\rho} + gh_{ou} + \frac{g(z_{ou} - z_{ol})}{2}\right] \tag{15}$$

From (14) and (15) issues, that

$$w_{ou}^2 - w_{iu}^2 = w_{ol}^2 - w_{il}^2 \tag{16}$$

The further conclusions may be drawn using continuity equation for mass rate of flow:

- for duct u

$$w_{iu}\rho A_{iu} = w_{ou}\rho A_{ou} \tag{17}$$

from which

$$w_{iu} = w_{ou}(A_{ou}/A_{iu}) \tag{18}$$

and so

$$w_{ou}^2 - w_{iu}^2 = w_{ou}^2\left[1 - (A_{ou}/A_{iu})^2\right]; \tag{19}$$

- for duct l, respectively

$$w_{il}\rho A_{il} = w_{ol}\rho A_{ol} \tag{20}$$

$$w_{il} = w_{ol}(A_{ol}/A_{il}) \tag{21}$$

$$w_{ol}^2 - w_{il}^2 = w_{ol}^2[1 - (A_{ol}/A_{il})^2] \tag{22}$$

From (16) with consideration of (19) and (22)

$$w_{ou}^2[1 - (A_{ou}/A_{iu})^2] = w_{ol}^2[1 - (A_{ol}/A_{il})^2] \tag{23}$$

which for A_{iu}=A_{il} and A_{ou}=A_{ol} gives

$$w_{ou} = w_{ol} \tag{24}$$

From (16) one may get also

$$w_{iu} = w_{il} \tag{25}$$

Equality (24) states that there is no difference in either solution of the outlet velocity of pumped ideal liquid in the model of immovable rotor immersed in a liquid. For real liquid, as in this paper for electrolyte, assuming equality of specific friction works in opposite ducts, the $l_{fu} = l_{fl}$, equality (24) stands to ensue from the Conservation of Energy Law.

An approximate pressure distribution in a liquid along the vertical diameter placed in the plane x = const., for immovable rotor, is depicted in Fig. 7.

2.3. Course and results of experiments

Preliminary tests with the use of all cathodes in the same conditions, i.e. angular positioning, Reynolds, and Schmidt number, revealed small differences in mass transfer coefficient values obtained with the help of each of them. It could result from unavoidable – in praxis – a different state of surfaces of particular cathodes and sometimes may be of consequence of accidental impurities in the nickel. A sequence of the cathodes and differences in results were changing during basic activation of cathodes and during final activation with help of proper electrolyte. In each stage of experiment the results from cathode No II were higher than those from the other cathodes. This cathode was selected for basic experiments. Its supremacy over the next one was equal to (5.5 ÷ 5.0)%.

The static measurements were carried out for the four angular settings α of the cathode No II in a stream of electrolyte passing through an upper part of the two-spiral outlet manifold of the casing – settings: 0u, 1u, 2u, 3u and a lower part – settings: 0l, 1l, 2l, 3l,

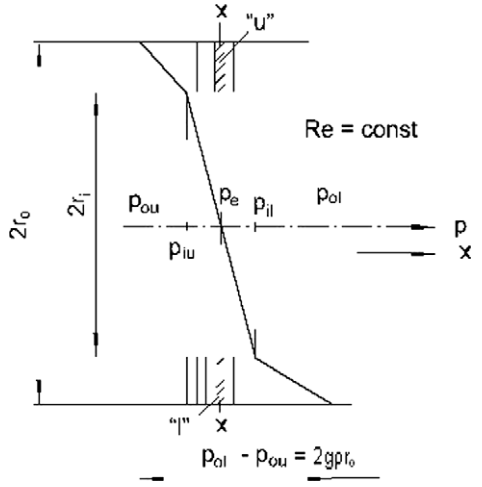

Fig. 7. Approximate pressure distribution in a liquid along the vertical diameter for immovable rotor.

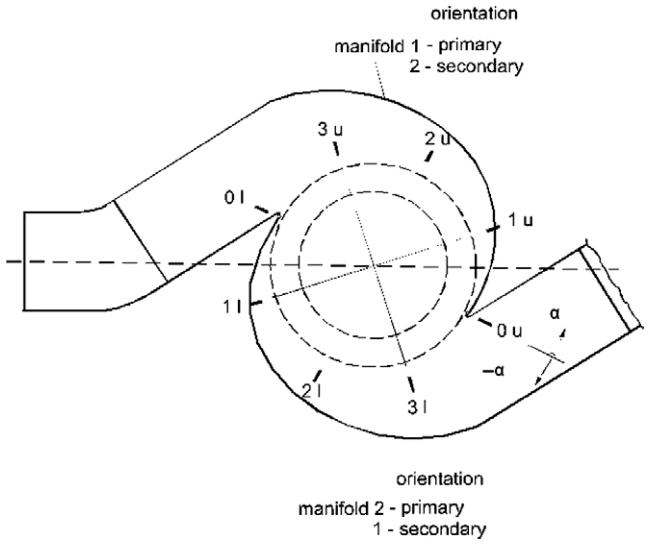

Fig. 8. Cathode positions every $\pi/4$ for primary and secondary orientations of manifolds.

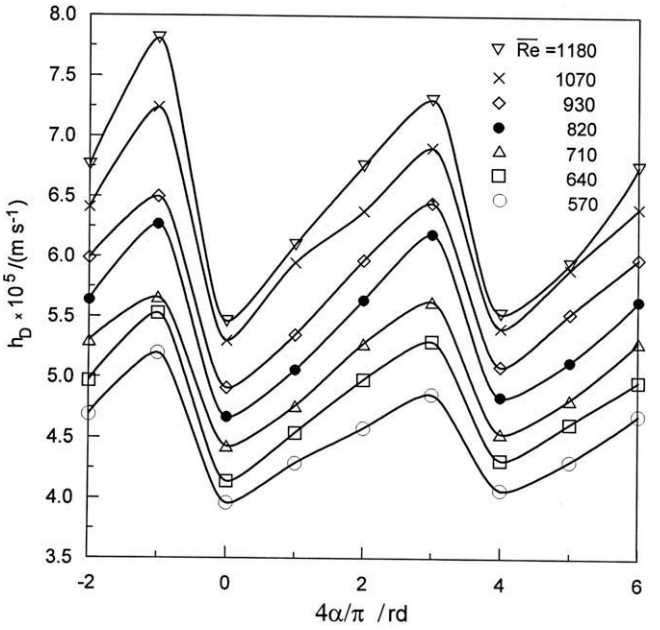

Fig. 9. Angular distribution of mass transfer coefficient at primary manifolds orientation.

which are marked every 45° in Fig. 8. The measurements were carried out for two orientations of manifold 1 and 2 also known as primary and secondary ones. The last was thought as a way to detect the influence of possible asymmetry of manifolds on the results of measurements.

As a parameter a mean Reynolds number was used and defined as

$$\overline{Re} = \overline{w}d/\nu, \tag{26}$$

where

$$\overline{w} = \dot{V}/(kA), \tag{27}$$

in which: A = $\Pi d^2/4$.

For the seven values of $\overline{Re}$ in the range between 570 and 1180-laminar flow through the ducts, the angular distribution of the mass transfer coefficient h_D, mean for the surface area of the cathode, was measured in the range $\alpha = 0$–2π. To this end the angle setting of cathode-axes was changed every $\pi/4$ rd, which corresponds to $4\alpha/\pi = 1$.

During direct measurements the electrolyte of $Sc = 1590$ was used. As a result the polarisation curves were obtained, on the basis of which plateaux currents could be stated. Distinguish were quite long segments of plateaux, characteristic for controlled diffusion at the cathode.

Mass transfer coefficient was calculated on the basis of the value of plateau current using the well-known equation

$$h_D = \frac{I_p}{nFA_{cath}C_b}, \tag{28}$$

where: $A_{cath} = \pi d\, L$, $n = 1$.

The ferricyanide ions concentration C_b was constant during the course of experiment and equal to 0.82×10^{-3} kmol m^{-3} for primary orientation of manifolds. The values obtained at primary orientation of manifold for all the angle settings of cathode at different values of $\overline{Re}$, made it possible to draw the graph presented in Fig. 9. The range $4\alpha/\pi$ from 0 to 4 refers to the manifold 1, whereas the remaining part of the graph refers to manifold 2. The values of h_D for $4\alpha/\pi$ equal 6 and −2, which also happen to equal themselves being specific for position 2*l* marked in Fig. 8. Distinct dependence of the heat transfer coefficient on the angle setting of the duct axes is visible on the graph. The higher Reynolds number, the greater amplitudes of changes of the coefficient.

A similar situation appeared after changing the orientation of manifolds on reverse one, for a certain value of ion concentration. The shape of the curves $I_p(\alpha)$ was, in substance, similar to those in Fig. 9. This testifies to the casing of the model. Further considerations apply to the primary orientation of manifolds.

On the basis of the known angle distribution of the mass transfer coefficient, presented in Fig. 9, a mean values of the mass transfer coefficient was calculated in the range $\alpha = (0$–$2\pi)$ rd or for $4\alpha/\pi$ in the range from −2 to 6, for each of the values of parameter $\overline{Re}$, using

$$\bar{h}_D = \frac{1}{2\pi}\int_0^{2\pi} h_D d\alpha \tag{29}$$

Then owing to

$$\overline{St}_M = \bar{h}_D/\overline{w} \tag{30}$$

and

$$\bar{j}_M = \overline{St}_M Sc^{2/3} \tag{31}$$

one could obtain the result presented in Fig. 10. They fit very well to the power dependence

$$\bar{j}_M = 0.456\overline{Re}^{-0.534} \tag{32}$$

In turn inserting (31) and (32) into (31) and considering (26) yields

$$\bar{w} = \left[\bar{h}_D \frac{(d/\nu)^{0.534} Sc^{2/3}}{0.456}\right]^{2.146} \tag{33}$$

which for: $d = 1$ mm, $\nu = 1.067 \times 10^{-6}$ m^2/s, $Sc = 1590$ results in

$$\bar{w} = 0.830 \times 10^9 \times (\bar{h}_D)^{2.146} \tag{34}$$

Next considerations were carried out under assumption that the correlation (34), in the range $\alpha = (0$–$2\pi)$ rd, stands approximately for $j_M = j_M(\mathrm{Re})$ in a range of real values of *Re*, in the duct, at fixed parameter $\overline{Re}$. In this connection the velocity $w(\alpha)$, at parameter $\overline{Re}$, could be calculated as

$$w(\alpha) = 0.830 \times 10^9 \times [h_D(\alpha)]^{2.146} \tag{35}$$

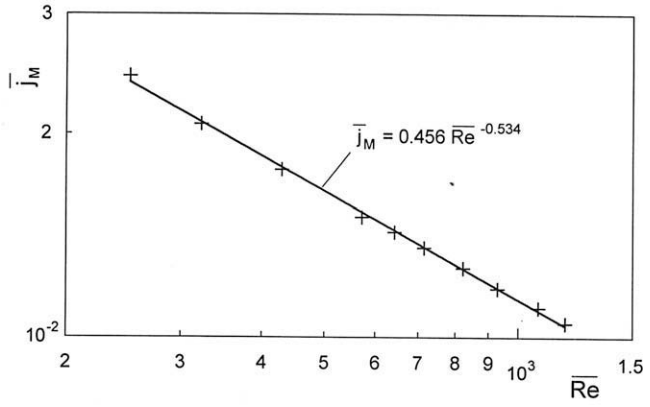

Fig. 10. Mean mass transfer Chilton-Colburn coefficient in static condition at primary orientation of manifolds.

In the correlation $h_D(\alpha)$ is known on the basis of direct measurements –Fig. 9.

The results of calculations of real values of *Re*, with the use of (35), were utilised for determining a deviation of *Re* in relation to $\overline{Re}$, defined as

$$\xi = (Re - \overline{Re})/\overline{Re}, \tag{36}$$

which graphically looks like in Fig. 11. Character of ξ a change that corresponds with that of the h_D change can be seen in Fig. 9. Maximum negative deviation refers to the duct-angle setting at which hydraulic resistance of flow of the electrolyte was the highest and vice versa. An absolute value of deviation was increasing with an increase of the parameter $\overline{Re}$. Maximum amplitude of the deviation occurred at $\overline{Re} = 1180$ and was equal to 85%.

The values of the arithmetic, mean deviation

$$\overline{\xi} = \frac{\sum_{i=1}^{7} \xi^i}{7} \tag{37}$$

of *Re* in relation to $\overline{Re}$, in an entire range of parameter $\overline{Re}$, at primary orientation of manifolds were contained in the range (−28 to 36)%.

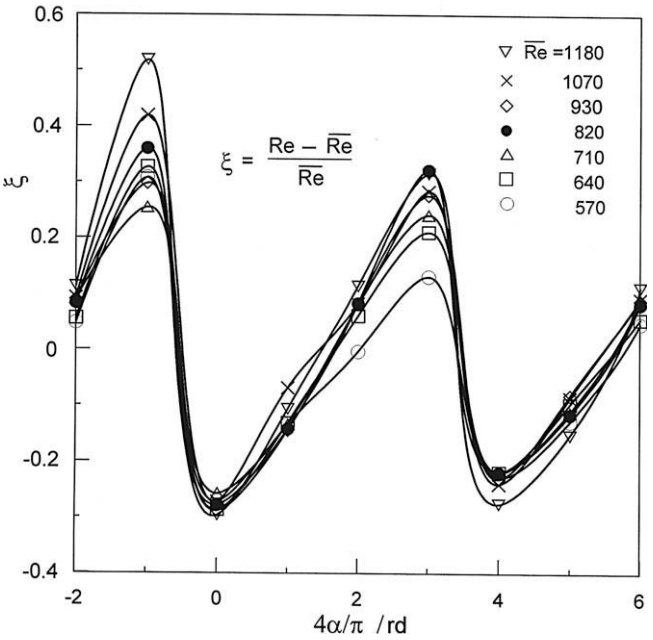

Fig. 11. Deviation of real Re in ducts, at an angle α, in relation to the mean $\overline{Re}$, at primary manifolds orientation.

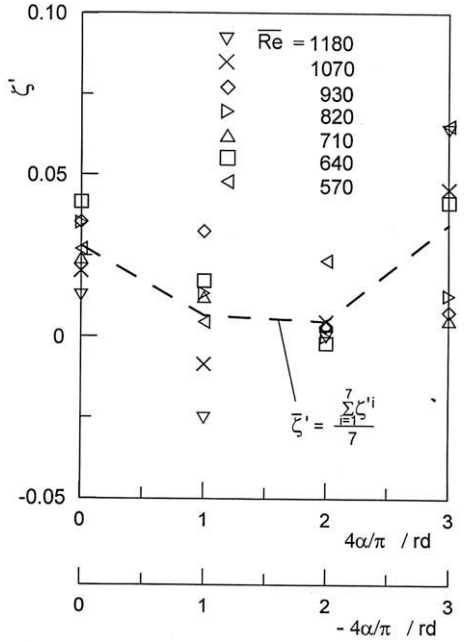

Fig. 12. Relative deviation of the mass transfer coefficient for opposite ducts, at primary manifolds orientation.

The results of direct experiments also enabled mutual deviation of results for the opposite ducts to be determined. The course of electrolyte in these ducts differed at π rd. To this end, for particular angle settings of opposite situated ducts, at parameter $\overline{Re}$, relative deviation of the value of mass transfer coefficient in lower duct from the value in the upper one was stated. The difference was related to the value for the lower duct. For both primary and secondary orientation of the manifolds was

$$\varsigma^j = (h^j_{Dl} - h^j_{Du})/h^j_{Dl}. \tag{38}$$

The results of calculations with use of (38) are presented in Figs. 12 and 13. One may notice, that the mean ς', i.e. the mean deviation of h'_{Dl} from the value h'_{Du} related to h'_{Dl}, with consideration of the range of $\overline{Re}$

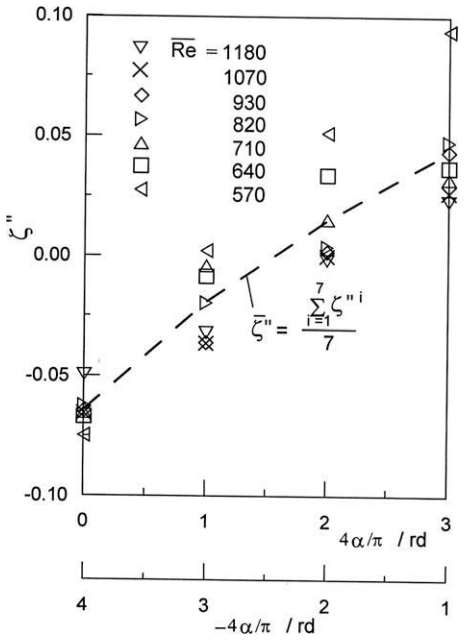

Fig. 13. Relative deviation of the mass transfer coefficient for opposite ducts, at secondary manifolds orientation.

Table 1
Uncertainty of determining of particular quantities.

Quantity	Relation	Value	Uncertainty	Relative uncertainty
$\bar{w}_{min}$	**(27)**	0.407 m s^{-1}	0.0273 m s^{-1}	0.067
$\bar{w}_{max}$		0.839 m s^{-1}	0.0562 m s^{-1}	
v	μ/ρ	1.067×10^{-6} m^2 s^{-1}	0.0267×10^{-6} m^2 s^{-1}	0.025
$\overline{Re}_{min}$	**(26)**	570	45	0.079
$\overline{Re}_{max}$		**1180**	**93**	
$I_{p\ min}$		$\mathbf{0.222 \times 10^{-3}}$ **A**	$\mathbf{0.001 \times 10^{-3}}$ **A**	0.005
$I_{p\ max}$		$\mathbf{0.426 \times 10^{-3}}$ **A**	**as above**	**0.002**
A_{cath}	$\Pi d\ L$	0.707×10^{-4} m^2	0.02×10^{-4} m^2	0.034
C_b	10^{-3} N V_t/V_s $[V_t] = [V_s] = ml$	0.82×10^{-3} kmol m^{-3}	0.04×10^{-3} kmol m^{-3}	0.049
$h_{D\ min}$	**(28)**	3.96×10^{-5} m s^{-1}	0.231×10^{-5} m s^{-1}	0.058
$h_{D\ max}$		$\mathbf{7.81 \times 10^{-5}}$ **m s^{-1}**	$\mathbf{0.454 \times 10^{-5}}$ **m s^{-1}**	
$\overline{St}_{M\ min}$	(30)	9.73×10^{-5}	0.866×10^{-5}	0.089
$\overline{St}_{M\ max}$		$\mathbf{9.31 \times 10^{-5}}$	$\mathbf{0.826 \times 10^{-5}}$	
Sh for $I_{p\ min}$	$h_D d/D$	88.5	6.7	0.076
Sh for $I_{p\ max}$		**174.6**	**13.2**	
Sc	v/D	1590	68	0.043
j_M for $I_{p\ min}$	**(31)**	13.3×10^{-3}	1.24×10^{-3}	0.094
j_M for $I_{p\ max}$		$\mathbf{12.7 \times 10^{-3}}$	$\mathbf{1.18 \times 10^{-3}}$	

is changing, according to the angle, from 0.5 to 3.5% at primary orientation of manifolds and ς'' is changing from −6.5 to 5% at secondary one.

Then the arithmetic mean of the above relative deviations $\bar{\varsigma}$

$$\bar{\varsigma} = (\bar{\varsigma}' + \bar{\varsigma}'')/2 \tag{39}$$

was used for preparation of Fig. 14. A value of the $\bar{\varsigma}$ is contained in the range of $(-2 \div 4)$% according to the angle α and amounted on an average about 0.4% in the range 2π of α.

This testifies to sufficient symmetry of the two manifolds of the model used and secondly confirms the theoretical inference on equality of electrolyte volume fluxes for both outlet manifolds in the case of closed, gas free hydraulic system.

2.4. Uncertainties of the results

A great influence of technical staff qualifications and especially its conscientiousness on uncertainties of results has been a specific feature of electrolytic research. Accurate testing equipment is necessary but not sufficient for successful research. Measurements are only a crowning achievement of usually long laborious efforts to prepare test section and the rig to be ready for running. There are many material-, technical-, process engineering- and performance requirements which have to be fulfilled for creating possibility of getting the reliable results. The last may be sometimes in part or entirely garbled because of only one slip. There is no quantitative measure for valuation of influence of laboratory faults and carelessness on the measuring results. This kind of uncertainty may only be minimised by following the verified laboratory procedures. Quite a lot of information on dealing with the laboratory problems, mentioned above, one may find in [6].

There is a classic average uncertainty of determining the final result for the composed quantities $y = f(x,z,u,\ldots)$ which one could present here. It is described by the relation

$$\Delta y = \sqrt{\left(\frac{\partial f}{\partial x}\Delta x\right)^2 + \left(\frac{\partial f}{\partial z}\Delta z\right)^2 + \left(\frac{\partial f}{\partial u}\Delta u\right)^2 + \cdots} \tag{40}$$

where

$\frac{\partial f}{\partial z}, \frac{\partial f}{\partial x}, \frac{\partial f}{\partial u}$, .. .– partial derivatives of function y in relation to the variable parameter, being specified in particular constituent measurement;

$\Delta x, \Delta z, \Delta u$, ... – mean uncertainties of particular measurements;

$\frac{\partial f}{\partial x}\Delta x, \frac{\partial f}{\partial z}\Delta z$, ... – partial uncertainties of intermediate measurements.

The results of calculations with use of (40) are presented in Table 1. They were collected using following data:

- for electrolyte at 25 °C [7]: D = (6.71± 0.23) × 10^{-10} m^2 s^{-1}, μ = (1.11 ± 0.03) × 10^{-3} kg m^{-1} s^{-1}, ρ = (1040 ± 5) kg m^{-3};
- for iodometric titration: N = 0.1 ± 0.0002, V_s = (25 ± 0.1) ml, $\Delta\dot{V}_t = \pm 0.01 ml$;
- other data: C = 0.974, d = 1.5 ± 0.05 × 10^{-3} m, L = (15 ± 0.1) × 10^{-3} m, $\Delta\dot{V}_r = \pm 2.8 \times 10^{-6}$ m^3 s^{-1}, F = 96 4935 × 10^3 As kmol^{-1}.

It is easy to notice that uncertainty of Sherwood number is given additionally for completing information.

An approximation uncertainty of results on $\bar{j}_M$ and $\overline{Re}$ with help of the straight line, seen in Fig. 14, may be omitted as the points lay very closely the line.

However, the uncertainty of correlation (32) may be stated as

$$\sqrt{\sum\left[\left(\frac{\Delta\bar{j}_M}{\bar{j}_M}\right)^2 + \left(\frac{\Delta\overline{Re}}{\overline{Re}}\right)^2\right]}. \tag{41}$$

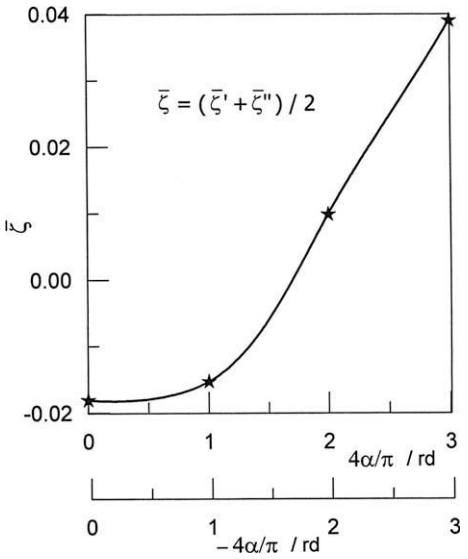

Fig. 14. Mean deviation of the mass transfer coefficient for radial, opposite ducts of the rotor model.

Assuming $\frac{\Delta j_M}{j_M} \approx \frac{\Delta j_M}{j_M}$ one gets the value of 0.123 on the basis of data in Table 1.

3. Conclusions

Angular inequality of liquid flow was stated in the ducts of the rotor of the model of regenerator in static conditions.

Electrolytic technique was proved to be useful in the experiment for measuring the mass transfer coefficient as quite distinct plateaux were characterising the polarisation curves in an entire range of Reynolds number.

The measured angle distribution of the mass transfer coefficient was utilised for getting the correlation on the mean, over round angle, Chilton–Colburn coefficient vs Reynolds number.

Approximate real angle-dependent velocity of electrolyte was calculated under assumption that the shape of dependence on it vs real mass transfer coefficient is the same as stated dependence on the mean velocity, over the whole rotor, vs mean mass transfer coefficient over the round angle.

Substantial deviations of real Reynolds number from its mean value, over the whole rotor, were revealed in the round angle.

Mutual equality – approximately – of the velocity of liquid in opposite ducts of the rotor, in a closed hydraulic system, was proved experimentally and justified theoretically.

Considering a scale of angle inequalities of velocity of liquid in rotor ducts, the phenomenon is worth to be taken into account in rotary regenerators design.

Acknowledgements

The author thank his co-workers Joanna Wilk for offering facilities to use the rotor with radial ducts and for help in carrying out initial experiments; Krzysztof Kiedrzyński and Bogusław Kasperski for their help in carrying out basic experiments and especially his granddaughter Natalia Gwiżdż, Guerin College Preparatory High School, River Grove, IL, USA, for linguistic proof-reading of the text.

References

[1] P.P. Grassmann, M. Tuma, Applications of the electrolytic method – II. Mass transfer within a tube for steady oscillating and pulsating flows, Int. J. Heat Mass Transfer 22 (1979) 799–804.
[2] T. Nishimura, N. Kojima, Mass transfer enhancement in a symmetric sinusoidal wavy – walled channel for pulsatile flow, Int. J. Heat Mass Transfer 38 (9) (1995) 1719–1731.
[3] T. Nishimura, S. Matsune, Mass transfer enhancement in a sinusoidal wavy channel for pulsatile flow, Heat Mass Transfer 32 (1996) 65–72.
[4] T. Moschandreou, M. Zamir, Heat transfer in a tube with pulsating flow and constant heat flux, Int. J. Heat Mass Transfer 40 (10) (1997) 2461–2466.
[5] Guo Zhixiong, Jin Sung Hyung, Analysis of the Nusselt number in pulsating pipe flow, Int. J. Heat Mass Transfer 40 (10) (1997) 2486–2489.
[6] B. Bieniasz, J. Wilk, Forced convection mass/heat transfer coefficient at the surface of the rotor of the sucking and forcing regenerative exchanger, Int. J. Heat Mass Transfer 38 (10) (1995) 1823–1830.
[7] M. Hopkowicz, Z. Pietrzyk, Pomiar współczynnika dyfuzji metodą wirującego dysku oraz dynamicznego współczynnika lepkości i gęstości dla układów $K_3Fe(CN)_6$–$K_4Fe(CN)_6$–NaOH, Inż. Chem. VII (4) (1977) 843–854 (in Polish) (Measurement of diffusion coefficient with use of the rotating disc method and of dynamic viscosity and density for systems $K_3Fe(CN)_6$–$K_4Fe(CN)_6$–NaOH).